Published in final edited form as:
Curr Biol. 2007 September 18; 17(18): 1586–1594.

Conditional disruption of intraflagellar transport in adult mice leads to hyperphagia-induced obesity and slow onset cystic kidney disease

James R. Davenport[1], **Amanda J. Watts**[2], **Venus C. Roper**[1], **Mandy J. Croyle**[1], **Thomas van Groen**[1], **J. Michael Wyss**[1], **Tim R. Nagy**[2], **Robert A. Kesterson**[3], and **Bradley K. Yoder**[1]

1 *Department of Cell Biology, University of Alabama at Birmingham*

2 *Department of Nutrition Sciences, University of Alabama at Birmingham*

3 *Department of Genetics, University of Alabama at Birmingham*

Introductory paragraph

The assembly of primary cilia is dependant on intraflagellar transport (IFT) which mediates the bidirectional movement of proteins between the base and tip of the cilium. In mice, congenic mutations disrupting genes required for IFT (e.g. *Tg737* or the IFT kinesin *Kif3a*) are embryonic lethal, while kidney-specific disruption of IFT results severe, rapidly progressing cystic pathology[1–3]. Although the function of primary cilia in most tissues is unknown, in the kidney they are mechanosenstive organelles that detect fluid flow through the tubule lumen [4]. Loss of this flow induced signaling pathway is thought to be a major contributing factor to cyst formation[5–7]. Recent data also suggest there is a connection between ciliary dysfunction and obesity as evidenced by the discovery that proteins associated with human obesity syndromes such as Alström and Bardet-Biedl localize to this organelle [8]. To more directly assess the importance of cilia in postnatal life, we utilized conditional alleles of two ciliogenic genes (*Tg737* and *Kif3a*) to systemically induce cilia loss in adults. Surprisingly, the cystic kidney pathology in these mutants is dependent on the time at which cilia loss was induced suggesting that cyst formation is not simply caused by impaired mechanosensation. In addition to the cystic pathology, the conditional cilia mutant mice become obese, are hyperphagic, and have elevated levels of serum insulin, glucose, and leptin. We further defined where in the body cilia are required for normal energy homeostasis by disrupting cilia on neurons throughout the CNS and on POMC-expressing cells in the hypothalamus, both of which resulted in obesity. These data establish that neuronal cilia function in a pathway regulating satiety responses.

Results

Our understanding of ciliary function in adults is hindered by the midgestation lethality of IFT mutants and severe near systemic pathology leading to early mortality in hypomorphic mutants [3,9,10]. To overcome this limitation, we utilized conditional null alleles of *Kif3a* and *Tg737* to systemically disrupt IFT using a tamoxifen-inducible Cre recombinase expressed from the actin promoter (CAGG-creER™[2,11,12]). Efficient deletion of *Tg737* and *Kif3a* and

Corresponding Author Bradley K. Yoder, MCLM 688, 1918 University Blvd, Department of Cell Biology, University of Alabama at Birmingham, Birmingham Alabama 35294 Phone: 205-934-0994, Fax: 205-934-0950, email: byoder@uab.edu.

subsequent loss of cilia was confirmed by Western blot and by immunofluorescence (Figure 1A and B). Despite the absence of cilia, the mutants did not exhibit cystic kidneys, hydrocephalus, or the ductal abnormalities in the pancreas or liver at 16 weeks post tamoxifen injection (Figure 1C–E, *ad libitum fed*) These phenotypes are normally p resent in the *Tg737*^{orpk} hypomorphic mutants where cilia function is impaired from conceptus [13–15]. Although there were no overt biliary duct phenotypes, there was a liver pathology that was evident in *ad libitum* fed mutants at 16 weeks post injection which consisted of an increase in lipid content as show by Oil Red O staining (Figure 1D and see below). This phenotype is not seen in the liver of the Tg737^{orpk} mutants. Cysts in the kidney and liver did eventually form in the conditional mutants. In the kidney, small cysts first became evident approximately six months after injection (Figure 1F). By one year, these cysts were severe and the kidneys had become markedly enlarged (Figure 1G). In contrast to the slow rate of cyst progression in the adult-induced mutants, administration of tamoxifen to pregnant females at E17.5 caused rapid cyst development in the kidney during the perinatal period normally within two weeks of birth (Figure 1H).

Although significant cystic pathologies in the kidney and liver were not seen in adult-induced cilia mutants until 6 months post tamoxifen administration, both male and female adult *Kif3a* and *Tg737* conditional mutants exhibit an increase in body weight shortly after tamoxifen administration (Figure 2A–D). In *Kif3a* and *Tg737* male and female mutants the weekly food intake was markedly increased compared to control mice (Figure 2E–F, Supplemental Figure 1A–B). The weight gain in these mutants was primarily due to hyperphagia as evidenced by the data from pair-feeding studies. While *Kif3a*$^{loxP/null}$; CAGG-creER™ (hereafter called Kif3a-cKO) mice fed *ad libitum* gained substantial weight, Kif3a-cKO mice pair-fed to the control (*Kif3a*$^{loxP/wt}$; CAGG-creER™, hereafter called Kif3a-cWT) did not exhibit a significant increase weight compared to controls (Figure 2G, Supplemental Figure 1C). In addition, we diet restricted Kif3a-cKO males to 4.0g food/day, similar to the food consumption by control littermates over a similar period and age. These mutants did not have significant changes in body weight compared to control littermates during the eight weeks of diet restriction; however, release of this diet restriction resulted in a rapid weight increase (Figure 2H).

Dual-energy X-ray absorptiometry (DXA) analysis of mice 14–16 weeks after tamoxifen administration indicated that both Kif3a-cKO males and females had significant increases in fat mass and percentage fat when fed *ad libitum*, while only minimal increases were seen in pair-fed mutants (Figure 3A, Supplemental Figure 1D). Post-mortem carcass analysis indicates that this gain in fat mass in *ad libitum*-fed mutants was observed across all fat pads examined (Figure 3B, Supplemental Figure 1E). Increased lean mass was also detected in Kif3a-cKO female mice (Supplemental Figure 1D); however, these changes were not seen after pair feeding.

The “systemic” loss of cilia in *Kif3a*$^{loxP/null}$ and *Tg737*$^{loxP/null}$ mutants fed *ad libitum* also resulted in elevated levels of leptin, as well as elevated fasting serum glucose and insulin similar to type II diabetes (Figure 3C–E and Supplemental Figure 2A–C). Levels of these hormones as well as fasting glucose were not elevated in pair-fed mutants, indicating the phenotype is a consequence of the obesity rather than a direct effect of cilia dysfunction.

In addition to increased adiposity, there were changes in organ weights in Kif3a-cKO mice after tamoxifen administration (Table 1). In *ad libitum*-fed mutants (16 weeks post tamoxifen injection), the livers and kidneys were nearly double the weight of controls. This was not seen in any of the pair-fed mice indicating these phenotypes are secondary consequence of the obesity and not due directly to loss of cilia. The increase in liver weight in the *ad libitum*-fed mutants was associated with lipid accumulation as reveled by Oil-red-O staining (hepatic

steatosis, Figure 1D, Supplemental Figure 2E– F). Histological analysis indicates that the increased kidney weight at 16 weeks post injection in the obese mice was not due to the increased cystogenesis specifically in the *ad libitum*-fed Kif3a-cKO mutants.

The hyperphagia-induced obesity observed after tamoxifen administration in adult mice raised the possibility the abnormal feeding behavior may be due to loss of ciliary function on neurons. To test this hypothesis, we crossed the conditional cilia mutants with the synapsin1-cre (Syn1-cre) mice. Although it did not occur as rapidly as seen for the CAGG-Cre line, both male and female cilia mutants generated with Syn1-cre become obese (Figure 4). The cause of the delayed phenotype relative to what is seen in the CAGG-CreER™ induced mutants is uncertain but may reflect differences in the efficacy of the Syn1-Cre or possibly indicate additional roles for cilia in energy homeostasis outside of the CNS.

To further define on which neurons cilia function is needed, we disrupted cilia on pro-opiomelanocortin (POMC)-expressing cells in the hypothalamus. This was accomplished by crossing the *Kif3a* conditional mutant with the POMC-cre deletor line [16,17]. To determine whether cilia were present on POMC neurons, we first crossed the Kif3a flox allele onto the Z/EG cre reporter strain. These mice were used to generate the conditional mutant and control mice. Cilia were detected by immunofluorescence analysis using an antibody to monoglycylated tubulin[18] and the POMC neurons by GFP expression. The data confirm that there is a single cilium present on most if not all POMC neurons (GFP^+) as well as most other cells in the hypothalamus (Figure 5A). In contrast, cilia were largely absent from the GFP positive POMC neurons in the conditional mutants while non-GFP positive cell types in the hypothalamus retain a cilium (Figure 5B). Cilia were also retained in other regions of the brain outside of the hypothalamus in these mutants (data not shown) where POMC-cre is not expressed. Importantly, both male and female $Kif3a^{loxP/null}$; POMC-cre (hereafter called Kif3a-pomcKO) mice exhibited a significant increase in weight compared to their sex and age matched controls (Figure 5C). As seen for the CAGG-CreER™ or Syn1-cre line, the obesity was due primarily to hyperphagia (Figure 5D and data not shown). In addition, the level of hyperphagia and obesity in the POMC-cre mice was not as remarkable as seen in the CAGG-creER™ mice. It is unlikely that the phenotype is caused by a loss of POMC neurons as we could detect no overt changes in the number of GFP positive cells in the hypothalamus of the mutants on the Z/EG reporter background (Figure 5A and B). Another possible mechanism that could cause the obesity phenotype would be a change in activity. However, our analysis of the day-night movement patterns of male and female Kif3a-pomcKO mutants revealed no overt differences from that in controls (Supplemental Figure 3A–B).

As seen with the CAGG-CreER line, DXA analysis revealed that the Kif3a-pomcKO mutants had a significant increase in percentage body fat and an increase in lean mass (Figure 5E). The increase in lean mass is likely a secondary effect of the increased adiposity or due to a small increase in linear growth (Figure 5F). Kif3a-pomcKO mice also had elevated levels of serum leptin and insulin and slightly higher blood glucose (Figure 5G–I). Oil-red-O staining again revealed hepatic steatosis. As seen with the conditional mutants generated with the CAGG-Cre line, the hepatic steatosis is a secondary effect of the obesity as this phenotype is not seen in pair-fed mutants and POMC-cre is not expressed in the liver (Supplemental Figure 3E–F).

Discussion

Cilia function is thought to be required for normal renal physiology as evidenced by the fact that disruption of cilia specifically in the developing kidney results in severe cystic disease [1,19]. Renal cilia have been shown to function as mechanosensor that detects fluid movement through the lumen of the nephron and loss of this mechanosensory activity is thought to be a key factor leading to cystogenesis[5–7]. Thus, it was surprising that the rate of cyst formation

was so attenuated after cilia were ablated in the adult mice compared to what occurs in the perinatal period. The difference in the cystic phenotype is not due to limited cre activity as immunofluorescence and Western blot analysis demonstrate a dramatic loss of cilia on renal tubules along with a reduction in *Kif3a* and *Tg737* protein levels well before the cystic pathology develops. The cause of the switch from a very aggressive cystic disorder in cilia mutants induced during renal development to a mechanism of slow cyst formation in adult is still being assessed. It remains a formal possibility that the large kidney cysts that develop in the adult induced mutants at 16 months post tamoxifen injection are related to the severity of obesity as is the case for the hepatic steatosis and glucose homeostasis abnormalities. We are currently addressing this issue using a kidney specific tamoxifen inducible Cre line. Overall, we believe the data indicate that renal cyst formation, as is likely the case for the pancreatic and hepatic ductile abnormalities associated with the cilia mutants such as $Tg737^{orpk}$ [13,14, 20], requires more than just loss of a pathway regulated by cilia-mediated mechanosensation.

In addition, our data show that loss of cilia in adult mice alters their feeding behavior and results in obesity with a phenotype resembling insulin resistance and diabetes. Obese mutants also exhibit renal hypertrophy, which is seen in diabetic mouse models and human patients[21, 22]. We further demonstrate that the obesity phenotype can largely be recapitulated by deletion of cilia on neurons throughout the CNS and more specifically on POMC-expressing cells. Although POMC-cre is also expressed in the pituitary, it is likely that the phenotype is due to loss of cilia function in hypothalamic POMC neurons. This is based on the fact that an obesity phenotype is also seen in cilia mutants generated with the synapsin-I cre line [23]. Furthermore, we analyzed corticosterone levels in obese and pair fed mutants that would likely be associated with affects on the pituitary and detected no significant differences or correlations between obese and non-obese mutant or control mice (Figure 3F and Supplemental Figures 3D and 4G). Together, these data argue against cilia dysfunction on cells in the anterior pituitary as being the cause of the obesity.

Another interesting observation is that the phenotype of the cilia mutants generated with the POMC- or SynI-cre lines are not as severe as seen when cilia loss is induced systemically in adults. This could reflect a difference in the efficacy or time of expression of these cre lines or indicate the possibility that cilia have additional roles in energy balance outside of the CNS. Another possibility is that neuronal feeding circuits are able to compensate for congenic loss of cilia function during development but lack this capacity in adults after disruption of cilia.

Mutations in several cilia or basal body localized proteins have been implicated in rare human obesity syndromes such as Alström (ALMS) and Bardet-Biedl (BBS) [8,24]. There are multiple proteins involved in BBS and recent data indicate they function as a complex to regulate vesicular transport to the cilium[24]. The ALMS1 protein which is involved in human Alström syndrome is also located at the base of the cilium and disruption of ALMS1 caused truncation of the cilium[22]. Recently another gene involved in the obesity and skeletal defects observed in human patients with Carpenter Syndrome was identified as RAB23 [25]. RAB23 is a negative regulator of the hedgehog pathway that functions downstream of the hedgehog receptors smoothened and patched, as well as cilia/IFT proteins such as *Tg737* (IFT88). Although the pathway disrupted in Carpenter Syndrome patients or in which tissue loss of RAB23 leads to the obesity phenotype is unknown, these recent data raise the possibility that the increased adiposity in our conditional cilia mutants may be related to abnormalities in hedgehog signaling. Overall these data are supportive of a role for the ciliary/basal body in regulating feeding behavior. The control of feeding in mammals is complex and involves signals from diverse tissues such as the intestine, pancreas, adipose, and stomach[26,27]. In many cases these signals converge on the CNS and particularly on neurons in the hypothalamus. Our data is consistent with a role for cilia on the hypothalamic POMC neurons in reception or response to a satiety signal such as leptin or insulin and suggest that this may be disrupted in

the BBS or ALMS patients. An alternative possibility is that cilia are involved in a pathway connecting POMC neuronal projections to known reward circuitry in regions of the brain such as the ventral tegmental area as recently proposed for leptin and its receptor [27,28]. As such, our data provide a more comprehensive assessment of the cellular mechanisms controlling food intake in mammals, and could provide novel insights into one of the central satiety pathways in humans.

Materials and Methods

1. Mice

The *Kif3a* mice containing loxP or null alleles were obtained from Dr. L. Goldstein and were maintained on a C57BL/6 background[2].

The *Tg737* conditional mutant allele was generated such that exons 4–6 would be deleted upon Cre recombinase mediated excision resulting in a null allele[12]. The *Tg737* null allele used was generated by germ line deletion of the *Tg737* conditional allele. For all the studies in this manuscript, the conditional mutants were generated with the $Tg737^{flox/\Delta}$ or $Kif3a^{flox/\Delta}$mice since this would require only a single Cre excision event to generate the mutants. Identically treated $Tg737^{flox/WT}$ or $Kif3a^{flox/WT}$ mice carrying the Cre transgenic were used as the control animals unless stated otherwise. Nearly identical results were obtained with either the *Tg737* or *Kif3a* conditional mutant mice when crossed with the same Cre line and data are not always presented for both lines.

The CAGG-creER™ mice were obtained from Jackson Laboratories and were generated by Dr. A. McMahon[11]. They were maintained on a mixed C57BL/6 and FVB background. POMC-cre mice were obtained from Dr. G. Barsh and were maintained on a mixed C57BL/6 and FVB background[16]. All mice were maintained in accordance with IACUC regulations at the University of Alabama at Birmingham. Genotyping of mice was performed as described previously[29].

For induction of Cre activity in the CAGG-creER™ line, tamoxifen administration was performed for five consecutive days when CAGG-creER™ mice were between 8–12 weeks of age. Tamoxifen (Sigma, St. Louis, MO) dissolved in corn oil (Sigma) was administered IP at a dose of 6.0 mg/40 g body weight as described previously[11]. For induction of Cre activity in the CAGG-creER™ line in embryonic animals, one injection of tamoxifen was administered IP to the mother at 9.0 mg/40 g body weight.

2. Western Blot Analysis

Briefly, pancreas and brain tissues of *Kif3a* or *Tg737* mice were dounce homogenized in a 50 mM Tris (pH 7.2) buffer as described previously[14]. Kidney tissues from *Kif3a* or *Tg737* were homogenized using a PowerGen700 tissue homogenizer (Fisher Scientific, Pittsburgh, PA) in a 50 mM Tris (pH 7.5) buffer (adapted from [30]). Protein concentrations were determined using a DC protein assay kit (Bio-Rad, Hercules, CA, USA) according to the manufacturer's instructions. Equivalent amounts of protein lysate (20 μg) were separated by electrophoresis on SDS-PAGE gels and transferred to nitrocellulose (Nitrobind; Micron Separations, Westboro, MA, USA). Western blot analysis was performed using either mouse monoclonal antibody against Kif3a (diluted 1:1000, Covance, Berkeley, CA, USA) or Tg737/Polaris (GN1700, diluted 1:2500,[31]). The filters were washed and incubated with horseradish peroxidase-conjugated secondary anti-rabbit or anti-mouse antibodies (diluted 1:1500, Bio-Rad). Filters were washed four times in a 1× PBS/0.2% Tween-20 solution and HRP signal was detected using a Super-signal West Dura Chemiluminescence Kit (Pierce, Rockford, IL, USA).

3. Immunofluorescence Analysis

Tissue from kidney and pancreas was isolated from Tg737-cWT and Tg737-cKO mice and snap-frozen in Tissue Tek O.C.T. compound (Sakura Finetek USA, Inc., Torrance, CA, USA) as described previously. Forty micron sections from tissues were fixed in 3% paraformaldehyde for 1 hour at 20ºC and permeablized in 100% methanol for 30 minutes at −20°C. Sections were then blocked for 30 minutes and incubated for 3 hours at 20ºC with anti-acetylated alpha-tubulin mouse monoclonal antibody (Sigma, T6793) that was directly conjugated to FITC using the Aminolink Kit (Pierce Biotechnology, Rockford, IL) and then stained with Hoechst (1:1000, Sigma #33258) to visualize the nucleus. Slides were mounted and analyzed by confocal immunofluorescence microscopy using a Leica confocal microscope TCS SP unit (Leica Microsystems, Wetzlar, Germany) and the Leica imaging software.

Tissue from the hypothalamus in Kif3a-pomcWT and Kif3a-pomcKO mice on the Z/EG reporter background was isolated after perfusion of a 2% paraformaldehyde/PBS solution and then cryoprotected using a 2% PFA/30% sucrose solution diluted in PBS. Free-floating sections (30 μm) were blocked and stained with TAP952 (1:100,000), a mouse monoclonal antibody directed against anti-monoglycylation of tubulin and visualized using a rhodamine red anti-mouse IgG secondary antibody (1:5000, Jackson Labs, Bar Harbor, ME)[18]. The rest of the process is described above.

4. Body Weight and Feeding Studies

All body weights from mice were measured between 5:00 pm to 6:00 pm weekly using a Mettler-Toledo digital weight scale (Columbus, OH). All animals undergoing food intake analysis studies were individually caged and food intake measurements were conducted weekly between 5:00–6:00 pm by measuring food left in the food compartment of the cage, and any noticeable pieces of food within the cage. Animals were fed 11% fat breeders diet throughout the study (Harlin Foods).

For pair feeding studies, food consumption of the tamoxifen-induced Kif3a-cWT controls was measured daily, and this amount plus 0.05 g of food was given to pair fed mice prevent any error resulting in starvation. For the diet restriction studies, 4.00 +/− 0.10 g of food were given to both Kif3a-cWT and Kif3a-cKO mice after the initial tamoxifen administration. At eight weeks, the animals were then given access to unlimited food. Weights were measured as described above.

5. Serum Hormone Analysis

All animals were handled for several days prior to collection of serum to reduce effects caused by stress. Each individual animal was transported into an isolated room, decapitated without anesthesia, and trunk blood was collected. Serum was isolated by centrifugation (24 minutes at 2500 rpm at 4°C, followed by an additional 5 min at 2500 rpm at 4°C) and stored at −80°C until analysis. Serum leptin and corticosterone analysis was performed as described previously [32]. Insulin analysis was performed using 100 μL aliquots of serum with materials purchased from Linco Research Inc. (St. Charles, MO) and analyzed using a Ektachem DT II System (Johnson and Johnson Clinical Diagnostics, Rochester, NY) with the assistance of the Energy Metabolism/Body Composition Core in the UAB Clinical Nutrition Research Center.

6. Body Composition Analysis

All mice were analyzed for body composition between 22–25 weeks of age with assistance of the Small Animal Phenotyping Core in the UAB Clinical Nutrition Research Center. Animals were briefly anes thetized and placed under a PIXImus Dual-energy X-Ray absorptiometer (DXA, GE-Lunar, Madison, WI) in order to evaluate fat and lean mass. One week after DXA

analysis, animals were killed and individual tissues were isolated and weighed as described previously.

7. Serum Glucose Measurement

Kif3a-cWT and cKO mice were fasted for four hours at 16 weeks post initial tamoxifen administration (age 21–25 weeks). An initial measurement of fasting blood glucose was acquired from the tail vein. Blood glucose levels were then measured using an OneTouch Ultra Glucometer and OneTouch Ultra blood glucose test strips (Lifescan, Milpitas, CA, USA). All animals were handled several days prior to taking the serum glucose sample and all blood samples were measured in a separate room in order to minimize stress placed on the tested animals.

8. Histological Analysis

For all hematoxylin and eosin staining, pancreas and kidney tissues from mutant and wild type mice were isolated and fixed in formalin overnight at 4°C. The tissues were then sectioned and stained with H&E as described previously[14]. Hepatic tissues used for Oil-Red-O sections were isolated and snap frozen in Tissue Tek O.C.T. compound (Sakura Finetek U.S.A.) as described above. Sections of the liver were then stained as described previously[33]. Images of tissues were captured on a Nikon TE200S microscope (Melville, NY) using a Micropublisher 3.3RTV camera (Burnaby, BC, Canada) and Q-imaging software.

9. Body Length Measurement

Immediately after DXA analysis when the animal was still anesthetized, ventral measurements from the tip of the nose to the middle of the anus (to the nearest 0.1 cm) were taken by two independent observers unaware of the genotypes. These measurements were averaged, and this value was then used in statistical analysis to calculate body length.

10. Activity Measurements

For long term locomotive activity, independent cages with a camera system (detecting infrared) recorded animal activity over a 24 hour period. The system consists of four home cages (30 ×30 cm) with a camera in the center of the top of each cage. The animal is put in the arena, is acquainted with the home cage for 24 hours and then observed for 24 hours, with a camera-driven tracker system (Phenotyper, Noldus, The Netherlands). The test measures the circadian activity pattern of the mice. The activity is measured on a 12:12 hour light/dark cycle, where the lights turn on at 6:00 and turn off at 18:00. Animals are provided a small black box home in the corner in order to sleep where movement is undetected by infrared light.

An open field maze was used for measuring short-term locomotive behavior and fear responses. The maze consists of an arena of 42 by 42 cm square with clear plexiglass sides (20 cm high). The animal is put in the arena, and observed for 5 min, with a camera-driven tracker system known as Ethovision (Noldus, The Netherlands). The arena is subdivided into three areas, the open center area, the sides, and the wall. The system records the position of the animal in the arena at 5 frames/second.

11. Statistical Analysis

All scientific graphs and statistical analysis were completed using OriginLab Software™ (Northhampton, MA). Either independent two-tailed student t-tests or one-way analysis of variance (ANOVA) analyses were used to calculate significant differences. In all cases, a value was deemed significant if $p<0.05$.

Supplementary Material

Refer to Web version on PubMed Central for supplementary material.

Acknowledgements

We would like to thank Dr. Maria S. Johnson from the University of Alabama at Birmingham (UAB) Small Animal Phenotyping Core for her assistance with the carcass analyses, Jinju Zhang from the UAB Transgenic Mouse Facility for his help with serum collection, and Dr. Barbara A. Gower and Maryellen Williams from the UAB Energy Metabolism and Body Composition Core for their help on the serum analyses. We would also like to thank Maya Watts, Jane Hosmer, and Camille Effler from the UAB Comparative Pathology Core for their technical support. We also would like to acknowledge Dr. Bré for her generosity in providing TAP952 antibody. BKY is supported by NIH R01DK65655, NIH R56DK075996, and the UAB Clinical Nutrition Research Center Pilot and Feasibility Project Grant. TRN and the UAB Small Animal Phenotyping Core are supported by UAB Clinical Nutrition Research Unit, P30DK56336; and the Alabama Neuroscience Blueprint Core Center, P30NS057098. RAK supported by NIH DK58382 and by NIH P30 CA13148 to UAB Transgenic Mouse Facility. The UAB behavioral core is supported in part by NIH P30 NS47466.

References

1. Lin F, Hiesberger T, Cordes K, Sinclair AM, Goldstein LS, Somlo S, Igarashi P. Kidney-specific inactivation of the KIF3A subunit of kinesin-II inhibits renal ciliogenesis and produces polycystic kidney disease. Proc Natl Acad Sci U S A 2003;100:5286–5291. [PubMed: 12672950]
2. Marszalek JR, Ruiz-Lozano P, Roberts E, Chien KR, Goldstein LS. Situs inversus and embryonic ciliary morphogenesis defects in mouse mutants lacking the KIF3A subunit of kinesin-II. Proc Natl Acad Sci U S A 1999;96:5043–5048. [PubMed: 10220415]
3. Murcia NS, Richards WG, Yoder BK, Mucenski ML, Dunlap JR, Woychik RP. The Oak Ridge Polycystic Kidney (orpk) disease gene is required for left-right axis determination. Development 2000;127:2347–2355. [PubMed: 10804177]
4. Singla V, Reiter JF. The primary cilium as the cell's antenna: signaling at a sensory organelle. Science 2006;313:629–633. [PubMed: 16888132]
5. Praetorius HA, Spring KR. The renal cell primary cilium functions as a flow sensor. Curr Opin Nephrol Hypertens 2003;12:517–520. [PubMed: 12920399]
6. Nauli SM, Alenghat FJ, Luo Y, Williams E, Vassilev P, Li X, Elia AE, Lu W, Brown EM, Quinn SJ, Ingber DE, Zhou J. Polycystins 1 and 2 mediate mechanosensation in the primary cilium of kidney cells. Nat Genet 2003;33:129–137. [PubMed: 12514735]
7. Al-Bhalal L, Akhtar M. Molecular basis of autosomal dominant polycystic kidney disease. Adv Anat Pathol 2005;12:126–133. [PubMed: 15900113]
8. Li G, Vega R, Nelms K, Gekakis N, Goodnow C, McNamara P, Wu H, Hong NA, Glynne R. A Role for Alstrom Syndrome Protein, Alms1, in Kidney Ciliogenesis and Cellular Quiescence. PLoS Genet 2007;3:e8. [PubMed: 17206865]
9. Davenport JR, Yoder BK. An incredible decade for the primary cilium: a look at a once-forgotten organelle. Am J Physiol Renal Physiol 2005;289:F1159–1169. [PubMed: 16275743]
10. Takeda S, Yonekawa Y, Tanaka Y, Okada Y, Nonaka S, Hirokawa N. Left-right asymmetry and kinesin superfamily protein KIF3A: new insights in determination of laterality and mesoderm induction by kif3A-/- mice analysis. J Cell Biol 1999;145:825–836. [PubMed: 10330409]
11. Hayashi S, McMahon AP. Efficient recombination in diverse tissues by a tamoxifen-inducible form of Cre: a tool for temporally regulated gene activation/inactivation in the mouse. Dev Biol 2002;244:305–318. [PubMed: 11944939]
12. Haycraft CJ, Zhang Q, Song B, Jackson WS, Detloff PJ, Serra R, Yoder BK. Intraflagellar transport is essential for endochondral bone formation. Development 2007;134:307–316. [PubMed: 17166921]
13. Banizs B, Pike MM, Millican CL, Ferguson WB, Komlosi P, Sheetz J, Bell PD, Schwiebert EM, Yoder BK. Dysfunctional cilia lead to altered ependyma and choroid plexus function, and result in the formation of hydrocephalus. Development 2005;132:5329–5339. [PubMed: 16284123]

14. Zhang Q, Davenport JR, Croyle MJ, Haycraft CJ, Yoder BK. Disruption of IFT results in both exocrine and endocrine abnormalities in the pancreas of Tg737(orpk) mutant mice. Lab Invest 2005;85:45–64. [PubMed: 15580285]
15. Pazour GJ, Dickert BL, Vucica Y, Seeley ES, Rosenbaum JL, Witman GB, Cole DG. Chlamydomonas IFT88 and its mouse homologue, polycystic kidney disease gene tg737, are required for assembly of cilia and flagella. J Cell Biol 2000;151:709–718. [PubMed: 11062270]
16. Xu AW, Kaelin CB, Takeda K, Akira S, Schwartz MW, Barsh GS. PI3K integrates the action of insulin and leptin on hypothalamic neurons. J Clin Invest 2005;115:951–958. [PubMed: 15761497]
17. Novak A, Guo C, Yang W, Nagy A, Lobe CG. Z/EG, a double reporter mouse line that expresses enhanced green fluorescent protein upon Cre-mediated excision. Genesis 2000;28:147–155. [PubMed: 11105057]
18. Bre MH, Redeker V, Vinh J, Rossier J, Levilliers N. Tubulin polyglycylation: differential posttranslational modification of dynamic cytoplasmic and stable axonemal microtubules in paramecium. Mol Biol Cell 1998;9:2655–2665. [PubMed: 9725918]
19. Yoder BK, Mulroy S, Eustace H, Boucher C, Sandford R. Molecular pathogenesis of autosomal dominant polycystic kidney disease. Expert Rev Mol Med 2006;8:1–22. [PubMed: 16515728]
20. Yoder BK, Richards WG, Sweeney WE, Wilkinson JE, Avener ED, Woychik RP. Insertional mutagenesis and molecular analysis of a new gene associated with polycystic kidney disease. Proc Assoc Am Physicians 1995;107:314–323. [PubMed: 8608416]
21. Satriano J. Kidney growth, hypertrophy and the unifying mechanism of diabetic complications. Amino Acids. 2007
22. Lee MJ, Feliers D, Mariappan MM, Sataranatarajan K, Mahimainathan L, Musi N, Foretz M, Viollet B, Weinberg JM, Choudhury GG, Kasinath BS. A role for AMP-activated protein kinase in diabetes-induced renal hypertrophy. Am J Physiol Renal Physiol 2007;292:F617–627. [PubMed: 17018841]
23. Zhu Y, Romero MI, Ghosh P, Ye Z, Charnay P, Rushing EJ, Marth JD, Parada LF. Ablation of NF1 function in neurons induces abnormal development of cerebral cortex and reactive gliosis in the brain. Genes Dev 2001;15:859–876. [PubMed: 11297510]
24. Nachury MV, Loktev AV, Zhang Q, Westlake CJ, Peranen J, Merdes A, Slusarski DC, Scheller RH, Bazan JF, Sheffield VC, Jackson PK. A Core Complex of BBS Proteins Cooperates with the GTPase Rab8 to Promote Ciliary Membrane Biogenesis. Cell 2007;129:1201–1213. [PubMed: 17574030]
25. Jenkins D, Seelow D, Jehee FS, Perlyn CA, Alonso LG, Bueno DF, Donnai D, Josifiova D, Mathijssen IM, Morton JE, Orstavik KH, Sweeney E, Wall SA, Marsh JL, Nurnberg P, Passos-Bueno MR, Wilkie AO. RAB23 mutations in Carpenter syndrome imply an unexpected role for hedgehog signaling in cranial-suture development and obesity. Am J Hum Genet 2007;80:1162–1170. [PubMed: 17503333]
26. Badman MK, Flier JS. The gut and energy balance: visceral allies in the obesity wars. Science 2005;307:1909–1914. [PubMed: 15790843]
27. Fulton S, Pissios P, Manchon RP, Stiles L, Frank L, Pothos EN, Maratos-Flier E, Flier JS. Leptin regulation of the mesoaccumbens dopamine pathway. Neuron 2006;51:811–822. [PubMed: 16982425]
28. Hommel JD, Trinko R, Sears RM, Georgescu D, Liu ZW, Gao XB, Thurmon JJ, Marinelli M, DiLeone RJ. Leptin receptor signaling in midbrain dopamine neurons regulates feeding. Neuron 2006;51:801–810. [PubMed: 16982424]
29. Taulman PD, Haycraft CJ, Balkovetz DF, Yoder BK. Polaris, a protein involved in left-right axis patterning, localizes to basal bodies and cilia. Mol Biol Cell 2001;12:589–599. [PubMed: 11251073]
30. Wakayama T, Koami H, Ariga H, Kobayashi D, Sai Y, Tsuji A, Yamamoto M, Iseki S. Expression and functional characterization of the adhesion molecule spermatogenic immunoglobulin superfamily in the mouse testis. Biol Reprod 2003;68:1755–1763. [PubMed: 12606335]
31. Haycraft CJ, Banizs B, Aydin-Son Y, Zhang Q, Michaud EJ, Yoder BK. Gli2 and Gli3 localize to cilia and require the intraflagellar transport protein polaris for processing and function. PLoS Genet 2005;1:e53. [PubMed: 16254602]
32. Johnson MS, Onorato DP, Gower BA, Nagy TR. Weight change affects serum leptin and corticosterone in the collared lemming. Gen Comp Endocrinol 2004;136:30–36. [PubMed: 14980794]

33. Tolwani RJ, Hamm DA, Tian L, Sharer JD, Vockley J, Rinaldo P, Matern D, Schoeb TR, Wood PA. Medium-chain acyl-CoA dehydrogenase deficiency in gene-targeted mice. PLoS Genet 2005;1:e23. [PubMed: 16121256]

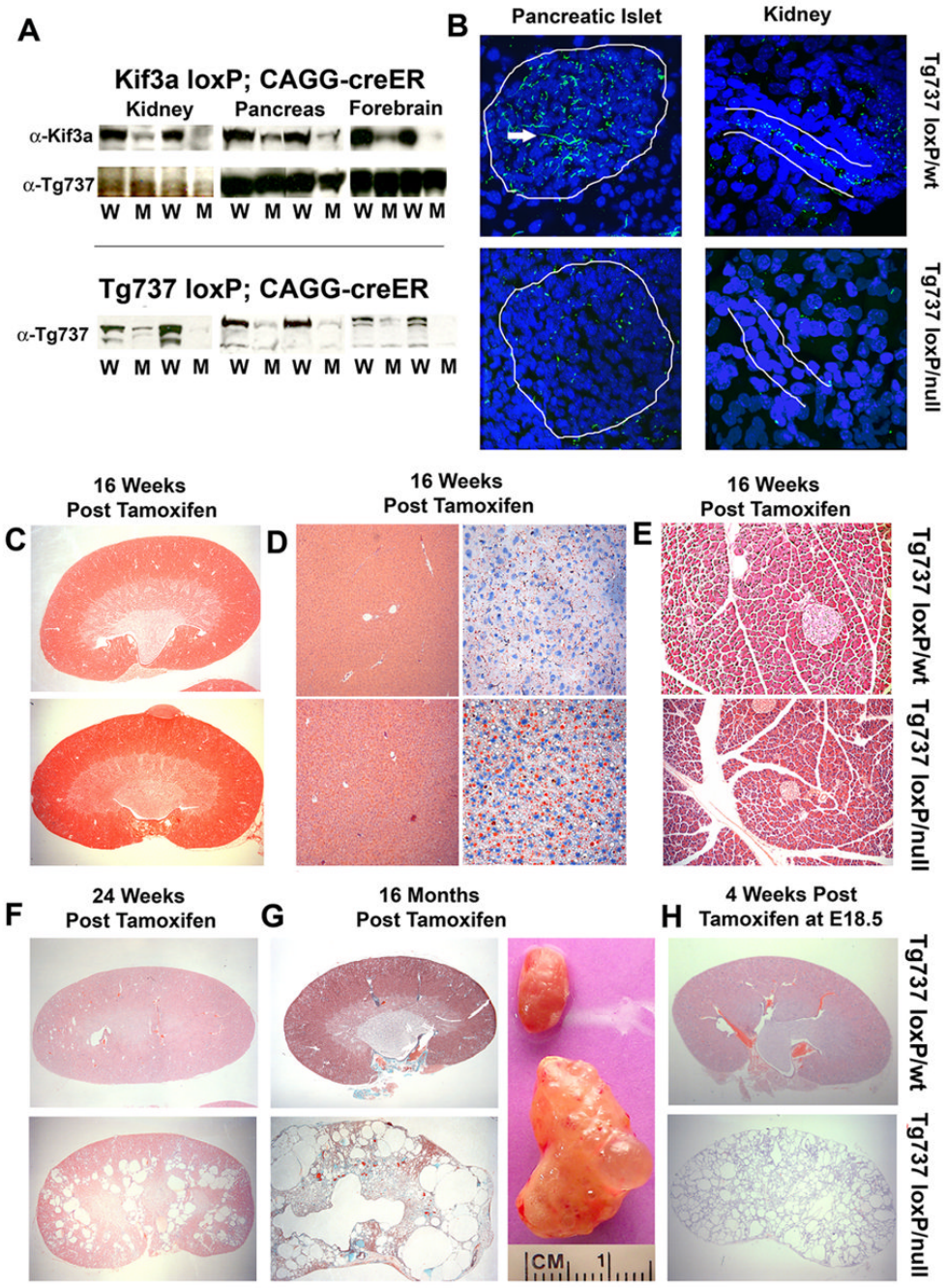

Figure 1. Systemic conditional deletion of Kif3a and Tg737 in adult mice leads to the development of slow onset cystic kidney disease

(A, top panel) Western blot analysis of Kif3a protein in kidney, pancreas, and brain in *Kif3a*$^{loxP/wt}$; CAGG-creER™ (W) and *Kif3a*$^{loxP/null}$; CAGG-creER™ (M) animals 16 weeks post tamoxifen administration. Tg737 protein expression (middle) was used as a loading control. (bottom panel) Tg737 protein expression was also measured in *Tg737*^{loxP}; CAGG-creER™ mutant (M) and control (W) kidney, pancreas, and brain. (B) Confocal immunofluorescence analysis of Tg737-cWT and cKO tissues demonstrate loss of cilia in the pancreatic islet (left panels; 63x; Tg737-cWT above, Tg737-cKO below) and in the nephrons of the kidney (right; 100x; Tg737-cWT above, Tg737-cKO below). The islet and tubule are

roughly outlined in white. The longer green staining pattern (pointed at by tip of white arrowhead) is due to background of the secondary antibody which reacts with an antigen on the vasculature and is unrelated to cilia. (C–E) Hematoxylin and Eosin (H&E) staining of (top) Tg737-cWT and (bottom) Tg737-cKO (C) kidney, (D, left panels) liver, and (E) pancreas at 16 weeks post tamoxifen administration in ad libitum fed mice shows no cystic pathology nor bile and pancreatic duct-related pathologies typical of the hypomorphic mutants at this age. Oil Red O staining (D right panels) shows an increase in lipid (red stain) accumulation in the mutants. (F) H&E staining of (top) Tg737-cWT and (bottom) Tg737-cKO kidneys at 24 weeks post tamoxifen injection in ad libitum fed mice revealed the development of cysts in Tg737-cKO mice (bottom). (G) Trichrome staining of (top) Tg737-cWT and (bottom) Tg737-cKO kidney sections 16 months post tamoxifen administration in ad libitum fed mice reveal the presence of very large cystic lesions throughout the kidney of the conditional mutants. Gross appearance of age and sex matched kidneys from Tg737-WT (top) and Tg737-cKO (bottom) are shown in the right panel. (H) H&E Staining of (top) Tg737-cWT and (bottom) Tg737-cKO kidney sections four weeks post administration of tamoxifen to the pregnant mother at embryonic day 18.5.

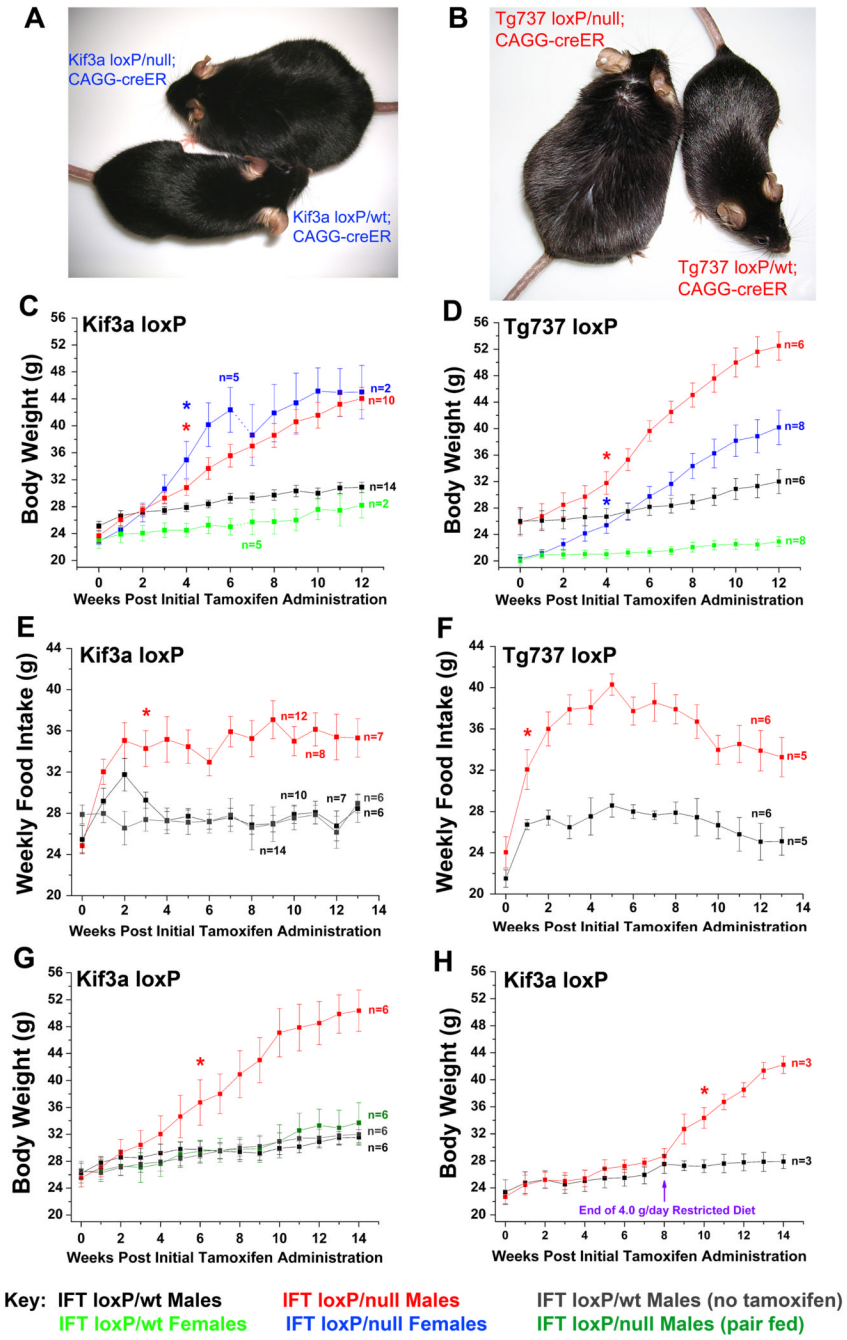

Figure 2. Systemic loss of Kif3a and/or Tg737 from adult mice results in a hyperphagia-induced obesity phenotype

(A) Images of Kif3a-cKO (left) and Kif3a-cWT (right) females 16 weeks after administration of tamoxifen. These littermates were of equivalent weight at time of injection. (B) Tg737-cKO (left) and Tg737-cWT (right) females are also shown 16 weeks after tamoxifen administration. (C,D) Body weight analysis of (C) Kif3a-cWT and Kif3a-cKO and (D) Tg737-cWT and Tg737-cKO males and females after tamoxifen administration (week zero). The number of Kif3a-cKO and Kif3a-cWT females analyzed in this study changed at week 6 when several of the mice were used to evaluate fat pad and organ weight masses. Animals were 8–12 weeks of age at the time of initial tamoxifen administration. (E,F) Weekly food intake analysis of (E)

Kif3a-cKO and Kif3a-cWT males and (F) Tg737-cKO and Tg737-cWT males after initial tamoxifen administration (week 0). Several animals were euthanized in the course of the experiment for body composition and histological analyses. Kif3a-cWT controls that were not induced with tamoxifen are also shown in blue (E). (G) Body weight analysis in pair feeding studies of Kif3a-cKO males after administration of tamoxifen. Separate groups of Kif3a-cWT males were tested with or without tamoxifen to assess changes due to tamoxifen administration. (H) Kif3a-cWT and Kif3a-cKO males were administered tamoxifen and were diet restricted to 4.0 g/day for 8 subsequent weeks. At 8 weeks, all mice were then fed *ad libitum* (* = $p \leq 0.05$, indicates the initial point of significant deviation between controls and mutants).

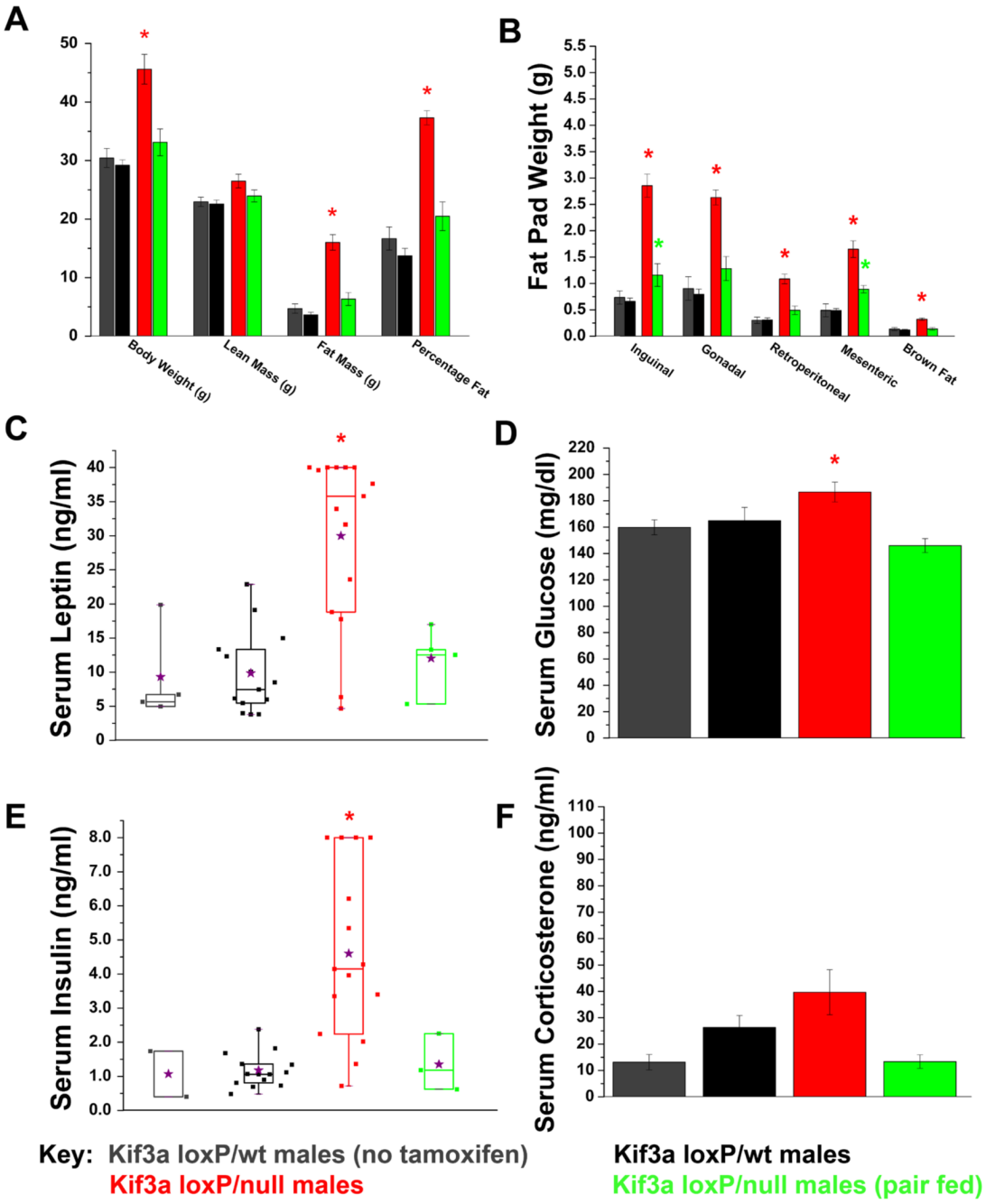

Figure 3. Body composition and serum analysis of the obesity phenotype displayed in Kif3a-cKO males

(A) Dual energy X-ray absorptiometry (DXA) displaying lean mass, fat mass, and percentage body fat of male Kif3a-cWT and Kif3a-cKO mice 14 weeks after initial tamoxifen administration. Body weight was measured immediately after the DXA. (B) Carcass analysis of various fat pads and brown fat in Kif3a-cWT and Kif3a-cKO males 16 weeks after initial tamoxifen administration. (C) Box and whisker plot of non-fasting serum leptin levels in Kif3a-cWT and KO males 16 weeks after initial tamoxifen administration. 8 of 10 Kif3a-cKO *ad libitum*-fed mice were above the maximum threshold of detection (40 ng/ml) and were assigned a value of 40 ng/ml. Mean serum leptin levels are indicated by purple stars. (D) Serum glucose

analysis of Kif3a-cWT and Kif3a-cKO males measured after 4 hours of fasting conditions. (E) Box and whisker plot of non-fasting serum insulin analysis of Kif3a-cWT and Kif3a-cKO males. 4 of 15 Kif3a-cKO males reached the highest detectable threshold for serum insulin analysis and were assigned the value of 8.0 ng/ml for statistical analysis. (F) Serum corticosterone analysis shows no significant differences between Kif3a-cWT and Kif3a-cKO males (* = $p \leq 0.05$, In (C) and (E), the means are indicated by the purple stars).

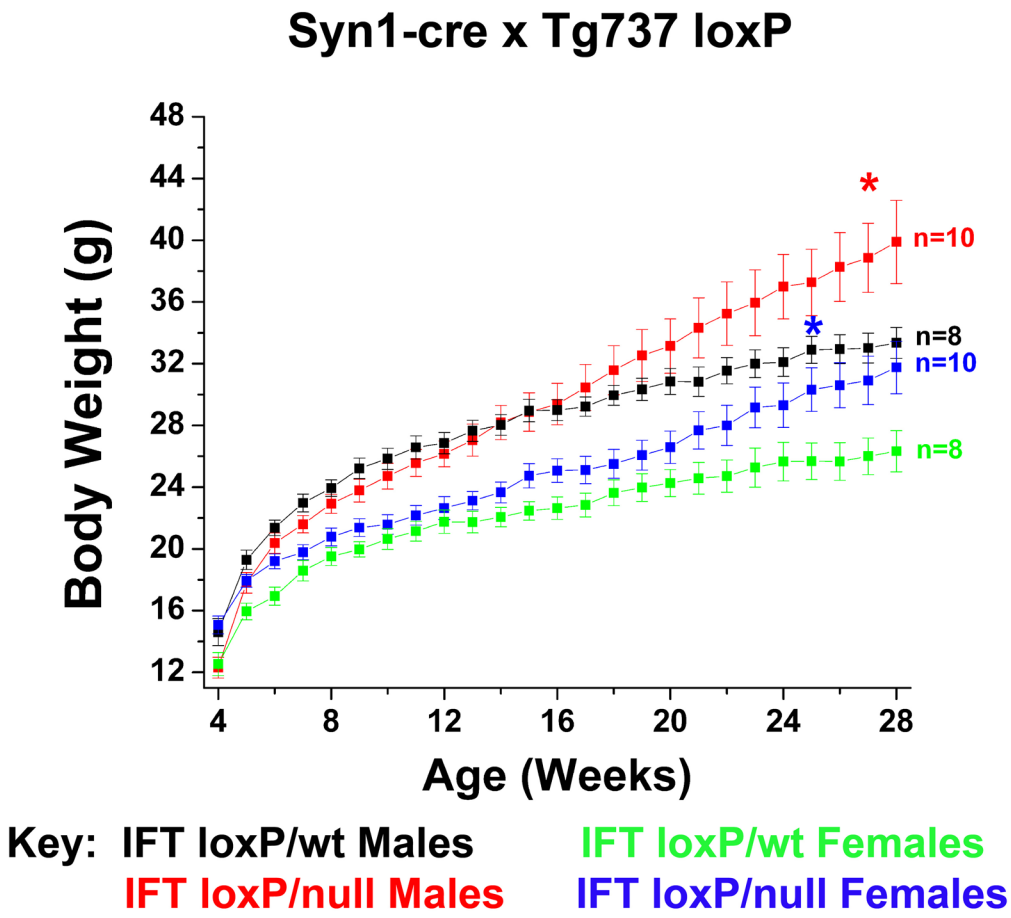

Figure 4. Conditional disruption of *Tg737* in neurons

Body weights of Tg737-syn1KO and Tg737-syn1WT male and female mice indicate that loss of neuronal cilia due to disruption of *Tg737* results in an obese phenotype.

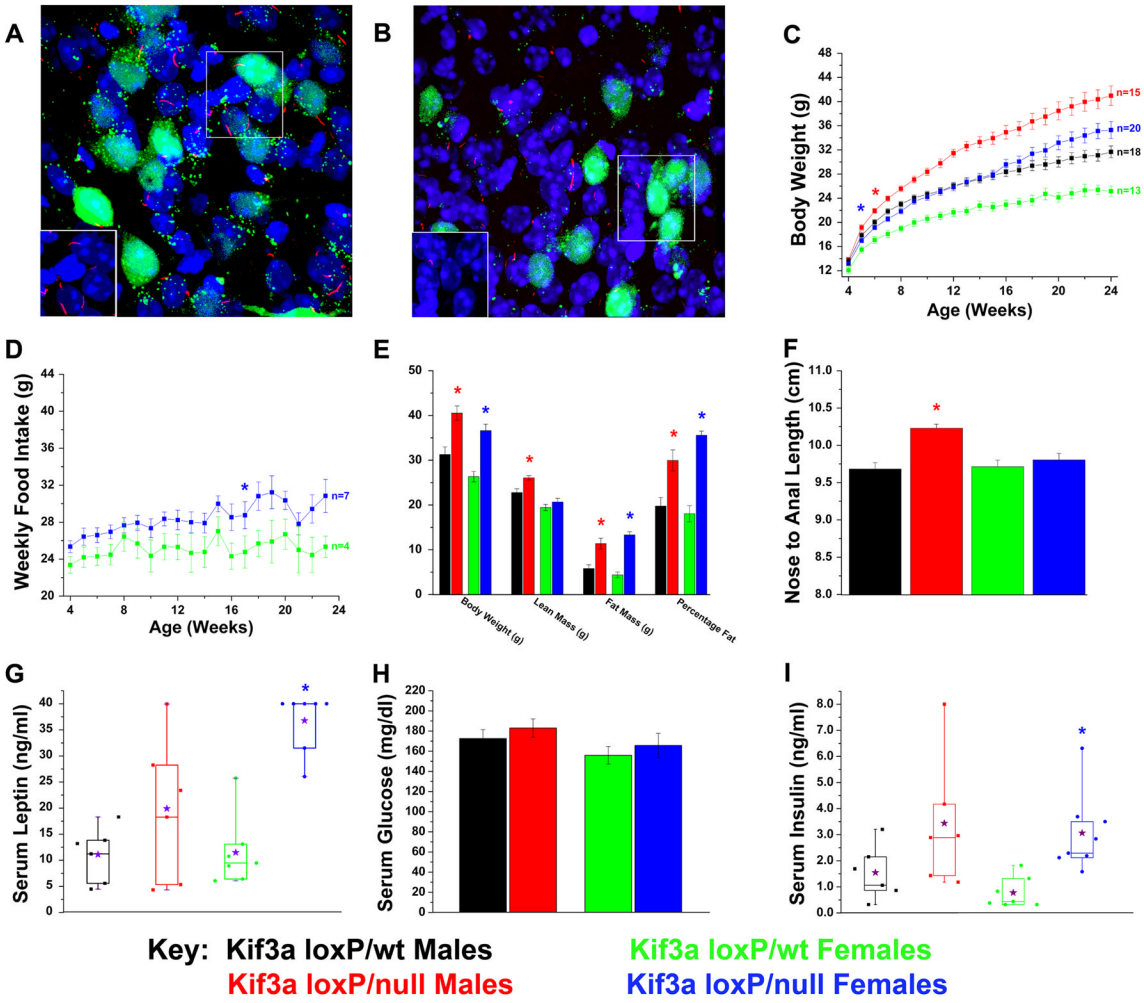

Figure 5. Conditional deletion of Kif3a from POMC-expressing cells in mice leads to increases in weight, adiposity, and body length

(A, B) Confocal immunofluorescence analysis of (A) *Kif3a*$^{loxP/wt}$ (Kif3a-pomcWT) and (B) *Kif3a*$^{loxP/null}$ (Kif3a-pomcKO) arcuate nucleus (100x) bred onto the Z/EG Cre reporter line in the presence of the POMC-cre deletor strain demonstrates the loss or stunting of neuronal cilia (red) on affected POMC neurons (green). Inserts show cilia (red) without the GFP signal and are derived from the boxed region in the image. Note that cilia are still retained on the non-POMC expressing cells in the hypothalamus. (C) Body weight analysis of Kif3a-pomcKO and Kif3a-pomcWT males and females. (D) Weekly food intake of Kif3a-pomcKO females was consistently increased from their Kif3a-pomcWT controls. (E) DXA analysis performed on adult (age 22–25 weeks) mice showed significant increases in fat mass and percentage fat in both sexes, and lean mass in male Kif3a-pomcKO mice. Body weight was measured after the DXA analysis. (F) Nose-to-anal length analysis conducted in anesthetized adult (age 22–25 weeks) Kif3a-pomcWT and Kif3a-pomcKO mice. The average length from independently determined two blinded measurements was used. (G–I) Serum analysis of (G) non-fasted leptin, (H) four-hour fasted glucose, and (I) non-fasted insulin in Kif3a-pomcWT and Kif3a-pomcKO mice (* = $p \leq 0.05$, in (C) and (D) indicating the initial point of significant deviation between controls and mutants. The purple stars in G and I represent the means of the individual groups.

Table 1

	Ad Libitum Fed			*Pair Fed*
	Kif3a loxP/wt; CAGG-creER Females (no tamoxifen) (n=4)	**Kif3a loxP/wt; CAGG-creER Females (n=7)**	**Kif3a loxP/null; CAGG-creER Females (n=7)**	**Kif3a loxP/null; CAGG-creER Females (pair fed) (n=4)**
Liver	1.266 +/− 0.067	1.139 +/− 0.067	2.424 +/− 0.295*	1.276 +/− 0.143
Kidney	0.292 +/− 0.017	0.300 +/− 0.016	0.730 +/− 0.295*	0.325 +/− 0.018
Pancreas	0.152 +/− 0.005	0.151 +/− 0.017	0.187 +/− 0.011	0.146 +/− 0.020
Heart	0.132 +/− 0.006	0.142 +/− 0.008	0.167 +/− 0.008*	0.116 +/− 0.007**
Ovary	0.011 +/− 0.001	0.013 +/− 0.001	0.014 +/− 0.001	0.014 +/− 0.002
Lung	0.213 +/− 0.025	0.227 +/− 0.011	0.257 +/− 0.033	0.196 +/− 0.024

* Organ weight significantly increased compared to controls ($p<0.05$).

** Organ weight significantly decreased compared to controls ($p<0.05$)